catalysts

MDPI

Article

Photocatalytic Activity and Stability of Organically Modified Layered Perovskite-Like Titanates $HLnTiO_4$ (Ln = La, Nd) in the Reaction of Hydrogen Evolution from Aqueous Methanol

Sergei A. Kurnosenko, Vladimir V. Voytovich, Oleg I. Silyukov, Ivan A. Rodionov and Irina A. Zvereva *

Department of Chemical Thermodynamics and Kinetics, Institute of Chemistry, Saint Petersburg State University, 199034 Saint Petersburg, Russia; st040572@student.spbu.ru (S.A.K.); st062003@student.spbu.ru (V.V.V.); oleg.silyukov@spbu.ru (O.I.S.); i.rodionov@spbu.ru (I.A.R.)
* Correspondence: irina.zvereva@spbu.ru

Abstract: Two series of hybrid inorganic–organic materials, prepared via interlayer organic modification of protonated Ruddlesden–Popper phases $HLnTiO_4$ (Ln = La, Nd) with *n*-alkylamines and *n*-alkoxy groups of various lengths, have been systematically studied with respect to photocatalytic hydrogen evolution from aqueous methanol under near-ultraviolet irradiation for the first time. Photocatalytic measurements were organized in such a way as to control a wide range of parameters, including the hydrogen generation rate, quantum efficiency of the reaction, potential dark activity of the sample, its actual volume concentration in the suspension, pH of the medium and stability of the photocatalytic material under the operating conditions. The insertion of the organic modifiers into the interlayer space of the titanates allowed obtaining new, more efficient photocatalytic materials, being up to 68 and 29 times superior in the activity in comparison with the initial unmodified compounds $HLnTiO_4$ and a reference photocatalyst TiO_2 P25 Degussa, respectively. The hydrogen evolution rate over the samples correlates with the extent of their interlayer hydration, as in the case of the inorganic–organic derivatives of other layered perovskites reported earlier. However, the $HLnTiO_4$-based samples demonstrate increased stability with regard to the photodegradation of the interlayer organic components as compared with related $H_2Ln_2Ti_3O_{10}$-based hybrid materials.

Keywords: photocatalysis; hydrogen; layered perovskite; titanate; intercalation; grafting

Citation: Kurnosenko, S.A.; Voytovich, V.V.; Silyukov, O.I.; Rodionov, I.A.; Zvereva, I.A. Photocatalytic Activity and Stability of Organically Modified Layered Perovskite-Like Titanates $HLnTiO_4$ (Ln = La, Nd) in the Reaction of Hydrogen Evolution from Aqueous Methanol. *Catalysts* **2023**, *13*, 749. https://doi.org/10.3390/catal13040749

Academic Editor: Marcos Fernández García

Received: 26 February 2023
Revised: 29 March 2023
Accepted: 11 April 2023
Published: 14 April 2023

1. Introduction

Overcoming many global ecological problems caused by the rapid industrial growth and the active use of traditional fuels in the XX–XXI centuries is associated with environmental remediation, the introduction of non-waste technologies and the development of alternative energy sources, including hydrogen. High calorific value and the absence of secondary pollution make hydrogen fuel a potential substitute for petroleum products and natural gas, which is of great importance in the context of the approaching energy crisis [1–3].

One of the environmentally friendly methods for producing hydrogen is known to be the photocatalytic decomposition of water and organic matter [4–7]. However, despite the recent advances in pure water splitting over powder semiconductor photocatalysts and in photoelectrochemical cells [8–10], the use of water as a raw for hydrogen generation still remains a major challenge for researchers due to thermodynamic and kinetic limitations of this reaction, which hinder the achievement of high quantum yields. In this regard, in recent years, much attention has also been paid to the photocatalytic conversion of plant biomass and its components (bioalcohols, carbohydrates, etc.) to produce hydrogen with much greater efficiency [11–19]. Moreover, the scientific community has begun the active

development of multifunctional photocatalysts for simultaneous hydrogen generation and environmental remediation via the decomposition of organic water pollutants [20–22].

At the moment, most investigated heterogeneous photocatalysts for plant biomass reforming are semiconductor oxides [23–29], sulfides [30,31], nitrides (primarily, metal-free g-C_3N_4 [32–34]), tungstates [35] and other compounds. Nevertheless, their photocatalytic activity often appears to be insufficient for implementation in industry, which motivates researchers to examine other types of photocatalytically active materials, including those with a layered type of structure. Among the latter, ion-exchangeable layered perovskite-like oxides deserve special attention due to their unique structural features and stability in aqueous and water–organic media. A crystal matrix of these oxides is formed by negatively charged perovskite slabs, alternating regularly with interlayer spaces occupied by different cations.

Remarkable photocatalytic activity of layered materials in relation to hydrogen generation, water purification and other reactions originates from the unique perovskite structure, being responsible for the efficient separation of photoexcited charge carriers and high chemical activity of the interlayer space towards intercalation and ion exchange [36–42]. In particular, the interlayer space is supposed to accommodate reactant molecules during photocatalytic reactions and, thus, serve as an additional reaction zone with new catalytic properties [43–45]. Furthermore, there are different approaches to the improvement of photocatalytic activity: ionic substitution in the perovskite slabs [46–51], surface tailoring with cocatalysts and photosensitizers [52–59], creation of heterojunctions [60–64], and exfoliation into nanosheets [65]. Another interesting approach to the modification of layered perovskite-like oxides is the introduction of organic components into the interlayer space, which allows producing hybrid inorganic–organic materials [66–68]. Organic modification is carried out either as intercalation of organic bases [69,70] or grafting of alcohols [71–73], carbohydrates [74], alkoxysilanes [75] and organophosphorus acids [76]. Despite a wide variety of known perovskite-based inorganic–organic derivatives, until recently, they were almost never investigated as catalysts or photocatalysts due to potential concerns about their stability under operating conditions [77]. However, our recent studies have shown that oxides $HCa_2Nb_3O_{10}$ and $H_2Ln_2Ti_3O_{10}$ (Ln = La, Nd), after organic modification, exhibit magnificent photocatalytic performance towards hydrogen production from aqueous methanol [78–82], glucose and xylose [83], being typical components of plant biomass processing. Particularly, the activity of the organically modified materials exceeded that of the initial protonated oxides up to 117 times, and apparent quantum efficiency reached 40% in the near-ultraviolet range after additional surface platinization. Despite the partial degradation of interlayer organic modifiers upon photocatalysis, the hydrogen evolution rate over the hybrid samples was found to be stable for a long time. The findings described made the creation of organically modified photocatalysts an intriguing and promising research direction. At the same time, it is important to note that all the aforementioned samples were based on n = 3 layered perovskites while the photocatalytic performance of such compounds is known to correlate with the perovskite slab thickness [77]. However, the activity of the materials with thinner perovskite slabs (particularly, n = 1) still remains a much less explored issue.

Layered perovskite-like compounds $HLnTiO_4$ are protonated forms of the Ruddlesden–Popper titanates $ALnTiO_4$ (A = alkali cation, Ln = La or lanthanide) whose structure is characterized by complete ordering of A^+ and Ln^{3+} cations between two nonequivalent interlayer spaces, separating perovskite slabs with a thickness of n = 1 titanium–oxygen octahedron (Figure 1) [84,85]. Unlike photocatalytic properties of the aforementioned n = 3 niobates and titanates, those of $ALnTiO_4$ are considered only in a few papers. Particularly, it was established that the activity of $ANdTiO_4$ in the reaction of aqueous methyl orange decomposition rises in the series of interlayer cations $A^+ = H^+$, Na^+, Li+ [86]. Photocatalytic properties of $HLnTiO_4$ (Ln = La, Nd) and the products of their topochemical dehydration in the reaction of hydrogen evolution from aqueous isopropanol were found to depend on a particular Ln^{3+} cation: La-containing samples provide a

2–4 times higher reaction rate than Nd-containing ones [87]. The activity of $KLaTiO_4$ in relation to pure water splitting was reported to increase after the partial substitution of Ti^{4+} by Zr^{4+} [47] and surface modification with Ni particles as a cocatalyst. Nitridation of $ALaTiO_4$ ($A^+ = K^+, H^+$), despite the bathochromic shift of the absorption edge, was found to result in the activity decrease because of pronounced electron-hole recombination on Ti^{3+} cations and surface defects as well as photodegradation of the nitrided compounds in general [50].

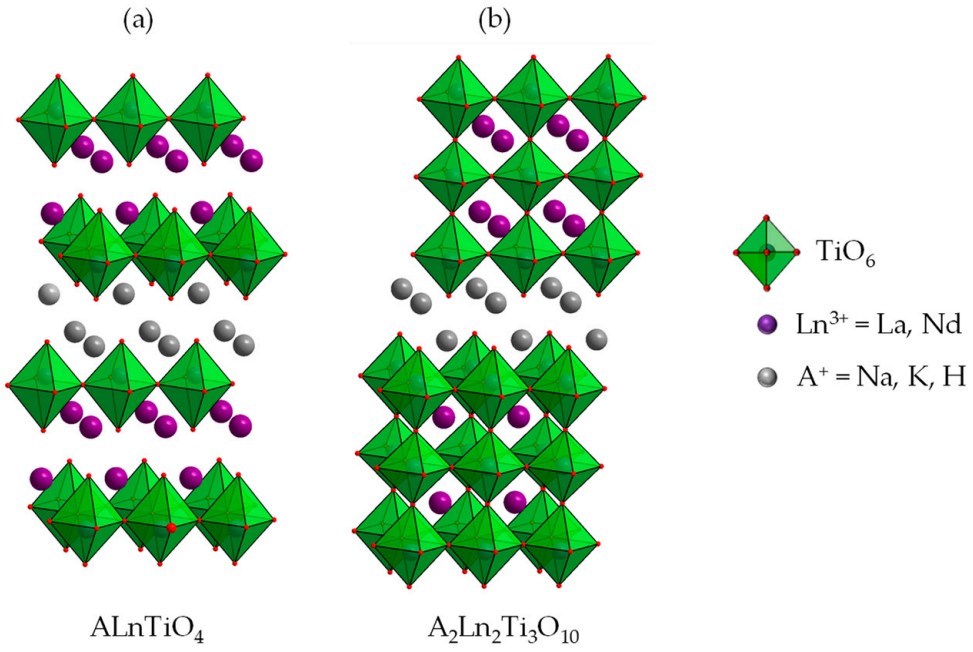

Figure 1. Structure of $ALnTiO_4$ (n = 1) (**a**) and $A_2Ln_2Ti_3O_{10}$ (n = 3) (**b**) titanates.

The present research continues the series of our articles on layered perovskite-based inorganic–organic photocatalysts and sheds light on the hydrogen evolution over the derivatives of relatively little-studied n = 1 titanates $HLnTiO_4$ (Ln = La, Nd) from aqueous methanol under near-ultraviolet irradiation for the first time. The study also pays attention to the further improvement of their photocatalytic activity via modification with a Pt cocatalyst and stability under operating conditions and makes a comparison of the n = 1 inorganic–organic samples with the related n = 3 compounds reported earlier.

2. Results and Discussion

2.1. Characterization of the Protonated and Organically Modified Titanates

The objects of the investigation are protonated titanates $HLnTiO_4$ (hereinafter designated as HLT for Ln = La and HNT for Ln = Nd) and their hybrid inorganic–organic derivatives $HLnTiO_4 \times RNH_2$ (HLT×RNH_2, HNT×RNH_2) and $HLnTiO_4 \times ROH$ (HLT×ROH, HLT×ROH) (R = methyl Me, ethyl Et, *n*-propyl Pr, *n*-butyl Bu, *n*-hexyl Hx, *n*-octyl Oc and *n*-decyl Dc) prepared via the intercalation of *n*-alkylamines and grafting of *n*-alcohols into the interlayer space. The above formulae of the inorganic–organic derivatives are only conventions for corresponding compounds, which do not reflect their true compositions.

All the aforementioned samples prepared for this photocatalytic study have been completely characterized in full accordance with the methods from our previous report [73]. Here, we highlight only the key points that are essential in the light of this research.

In accordance with the powder XRD data (Figure S1), both protonated titanates HLT and HNT, as well as all the products of their organic modification, were successfully prepared as individual phases not containing perceptible impurities. Tetragonal lattice parameters of HLT and HNT were determined to be a = 3.71 Å, c = 12.2 Å and a = 3.68 Å, c = 12.1 Å, respectively, which generally agrees with the literature data [85]. In both cases,

the *c* parameter is equal to the interlayer distance *d* (Table 1), and adjacent perovskite slabs are arranged in a staggered conformation in relation to the proton-populated interlayer space, which corresponds to the existence of a relative displacement of the perovskite slabs along both lateral axes by *a*/2. The *n*-alkylamine and *n*-alkoxy derivatives are distinguished from the background of the protonated titanates by the interlayer space significantly expanded by inserted organic components, which is clearly seen from the low-angle shift of the (00x) reflections and the corresponding increase in the *c* lattice parameter and interlayer distance *d*, being proportional to the organic chain length. As noted earlier [73], for all the organically modified titanates, the *c* parameter and interlayer distance *d* are related by the equality $c = 2d$, which points to the probable change of the perovskite slabs' conformation from staggered to eclipsed under the action of organic components being incorporated. At the same time, titanium–oxygen octahedra appear to preserve their lateral sizes since positions of some reflections, such as (110) and (020), as well as the *a* lattice parameter, stay predominantly unchanged upon the organic modification.

Table 1. Lattice parameters in the tetragonal system, interlayer distances *d*, organic (x) and water (y) content per formula unit, light absorption edges and specific surface areas of the initial titanates and their inorganic–organic derivatives. Compositions of the *n*-alkylamine and *n*-alkoxy derivatives are presented as $HLnTiO4{\cdot}xRNH_2{\cdot}yH_2O$ and $H_{1-x}LnTiO_{4-x}{\cdot}xRO{\cdot}yH_2O$, respectively.

Sample	*a*, Å	*c*, Å	*d*, Å	x	y	E_g, eV	λ_{max}, nm	S, m^2/g
HLT	3.71	12.2	12.2	–	0.05	3.45	359	9.7
×$MeNH_2$	3.77	33.3	16.7	0.35	0.45	3.58	346	4.0
×$EtNH_2$	3.75	37.7	18.9	0.35	0.50	3.48	356	–
×$PrNH_2$	3.76	41.2	20.6	0.35	0.30	3.50	354	–
×$BuNH_2$	3.76	47.8	23.9	0.40	0.25	3.61	343	2.6
×$HxNH_2$	3.76	54.9	27.5	0.35	0.45	3.47	357	–
×$OcNH_2$	3.78	66.3	33.2	0.45	0.40	3.49	355	15
×MeOH	3.72	32.3	16.2	0.70	0.45	3.47	357	17
×EtOH	3.72	36.6	18.3	0.40	0.50	3.47	357	–
×PrOH	3.73	41.6	20.8	0.45	0.35	3.45	359	–
×BuOH	3.73	45.6	22.8	0.40	0.25	3.45	359	1.6
×HxOH	3.74	55.4	27.7	0.40	0.10	3.46	358	–
×DcOH	3.73	56.8	28.4	0.35	0.05	3.46	358	6.4
HNT	3.68	12.1	12.1	–	0.10	3.48	356	8.5
×$MeNH_2$	3.74	33.1	16.6	0.35	0.40	3.41	364	5.6
×$EtNH_2$	3.74	37.6	18.8	0.45	0.20	3.50	354	–
×$PrNH_2$	3.74	40.4	20.2	0.45	0.40	3.43	362	–
×$BuNH_2$	3.74	47.7	23.9	0.45	0.30	3.50	354	5.6
×$HxNH_2$	3.72	54.0	27.0	0.45	0.35	3.42	363	–
×$OcNH_2$	3.81	65.4	32.7	0.45	0.40	3.45	359	7.7
×MeOH	3.71	32.0	16.0	0.75	0.40	3.42	363	5.0
×EtOH	3.70	36.4	18.2	0.50	0.30	3.39	366	–
×PrOH	3.72	41.1	20.6	0.40	0.15	3.45	359	–
×BuOH	3.71	44.5	22.3	0.40	0.15	3.45	359	4.0
×HxOH	3.71	54.9	27.5	0.40	0.10	3.41	364	–
×DcOH	3.71	58.0	29.0	0.35	0.10	3.41	364	15

As follows from the spectroscopic data [73], the *n*-alkylamine derivatives synthesized are non-covalent intercalation compounds with *n*-alkylammonium cations associated electrostatically with interlayer oxygen vertices of perovskite octahedra. The *n*-alkoxy derivatives, on the other hand, contain organic chains anchored covalently to the perovskite matrix. Along with organic components, all the organically modified samples preserve some amount of intercalated water (Table 1).

Diffuse reflectance spectra transformed into Tauc plots (Figures 2, S2 and S3) allow estimating optical bandgap energies E_g of the titanates under consideration (Table 1). As one

can see, light absorption by La-containing samples is only due to the interband transition occurring in the near-ultraviolet region whilst Nd-containing compounds also have visible absorption bands associated with energy transitions of f-electrons, which provides a purple color of the corresponding powders. Insertion of organic components into the interlayer space is found not to be accompanied by any changes in general spectrum appearance and visible absorption bands. However, upon the interlayer space expansion, the corresponding shift of bandgap energy reaches 0.16 eV, although it does not give an evident correlation with the organic chain length. The relatively weak influence of organic modifiers on the light absorption region is associated with the fact that energy bands in the materials in question are known to be formed by 2p-orbitals of oxygen and 3d-orbitals of titanium [88], which are not strongly affected by inserted organic modifiers. Thus, the operating range of the organically modified titanates as photocatalysts is middle- and near-ultraviolet. Taking into account the DRT-125 lamp spectrum (Figure S4), the differences in the long-wavelength absorption edge of HLT-based samples (Table 1) cannot be a weighty reason for those in their photocatalytic behavior since the lamp does not have emission peaks in the range of 343–359 nm. At the same time, the red absorption edge of some HNT derivatives is located near an intense lamp peak at 365 nm, which could provide greater photocatalytic reaction rates over these samples due to a wider range of available light. However, since this peak meets the absorption edge of the samples, the quantum yield of the reaction at this wavelength is hardly high enough. With that said, the possible absorption at 365 nm was not taken into account while calculating the quantum efficiency φ and, consequently, its value for some HNT-based samples may be somewhat overestimated.

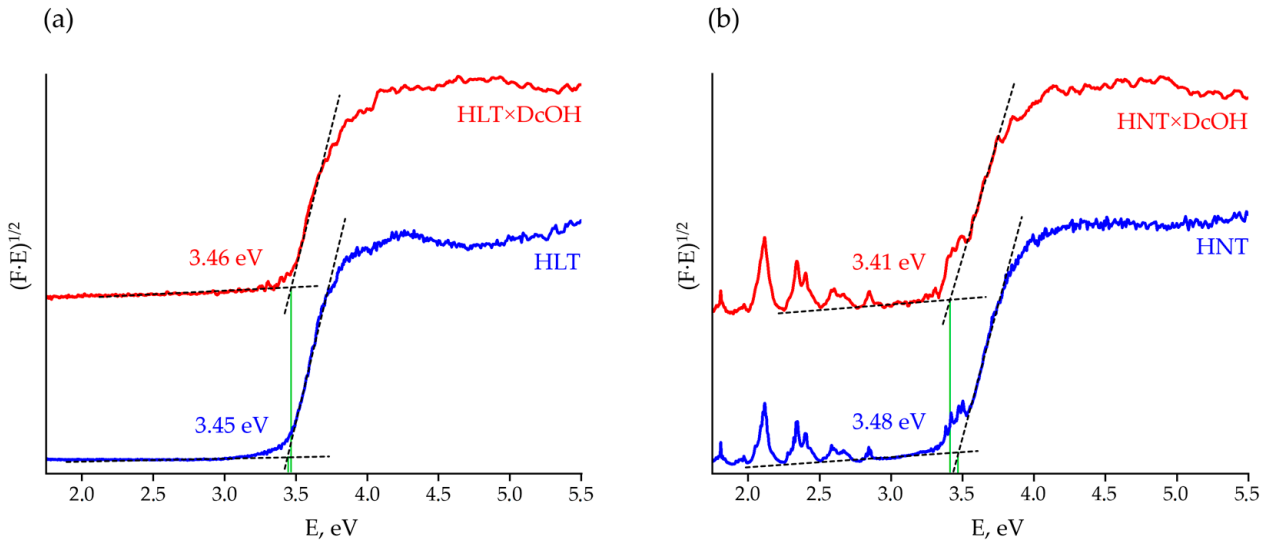

Figure 2. Tauc plots for the initial protonated forms and *n*-decoxy derivatives of HLT (**a**) and HNT (**b**) titanates.

The specific surface area of the titanates under study falls in the range of 1.6–17 m^2/g (Table 1). The large spread of its values, apparently, originates from the pronounced polydispersity of the samples' powders observed earlier in the SEM images [73,89], which, in turn, is predetermined by the high-temperature ceramic synthesis of the alkaline precursors, resulting in high crystallinity but strong accretion of the oxide polycrystals. Nevertheless, some organically modified $n = 1$ titanates (particularly, HLT×$OcNH_2$, HLT×MeOH, HNT×DcOH) turn out to show much greater specific surface areas in comparison with those of $n = 3$ titanates and niobates studied earlier [80,81].

2.2. Photocatalytic Activity of the Protonated and Organically Modified Titanates

Photocatalytic activity and stability of the titanates prepared were investigated in the reaction of light-driven hydrogen evolution from 1 mol. % aqueous methanol being

a typical biomass-derived compound. All the samples were tested both in a bare form and after modification with a 1% Pt cocatalyst. Along with reaction rates and apparent quantum efficiencies (Figures 3 and 4, Table S1), the photocatalytic measurements were aimed at monitoring the potential dark activity of the samples as well as the stability and composition of reaction suspensions (Tables S2 and S3).

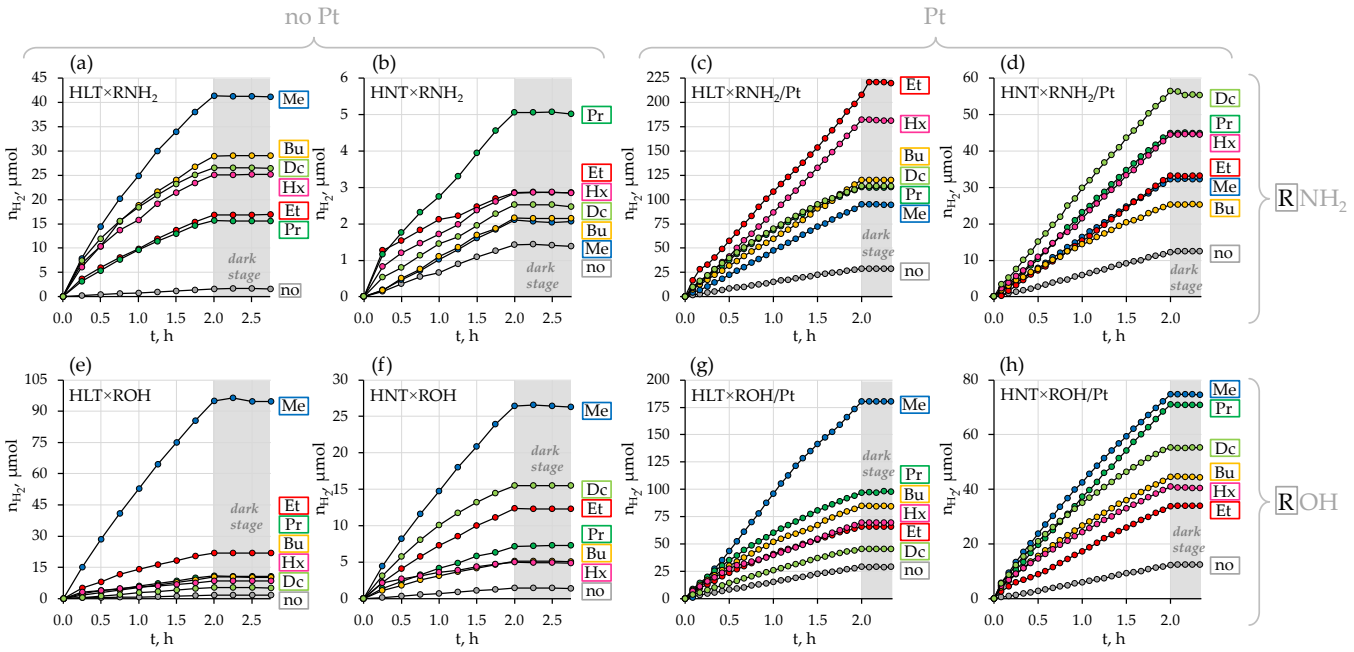

Figure 3. Kinetic curves of photocatalytic hydrogen evolution over the initial protonated titanates, their *n*-alkylamine (**a**–**d**) and *n*-alkoxy (**e**–**h**) derivatives in a bare state and with a Pt cocatalyst from 1 mol. % aqueous methanol under near-ultraviolet irradiation. Grey background corresponds to the dark stages (irradiation source is turned off).

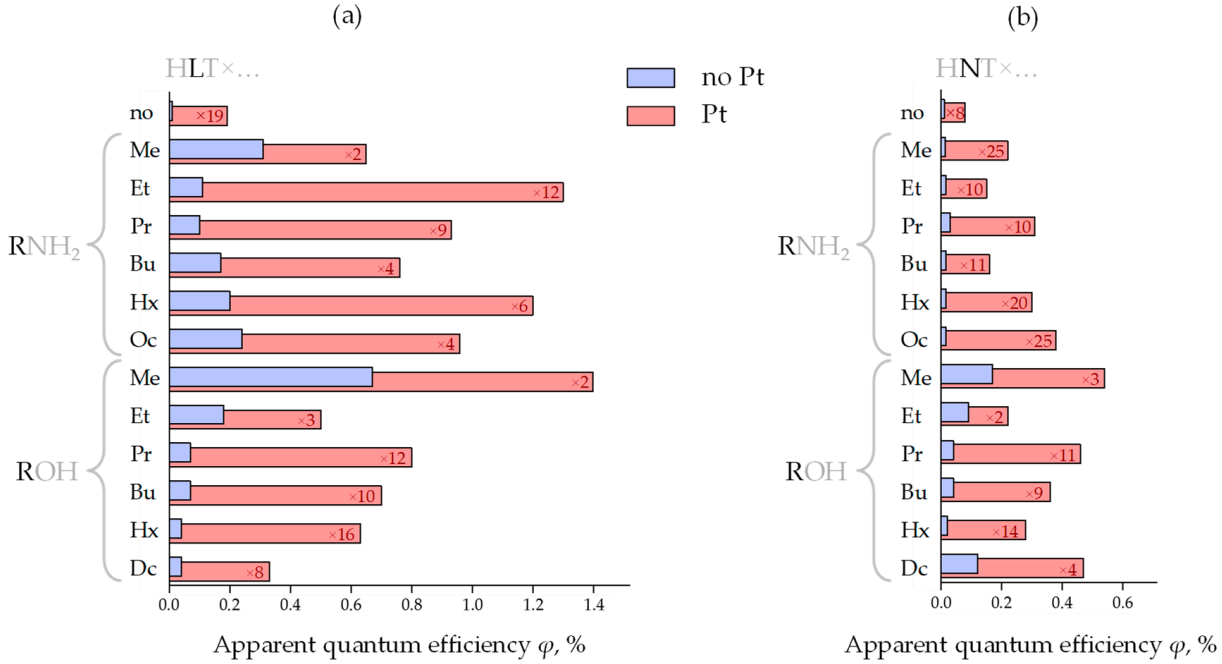

Figure 4. Apparent quantum efficiency of photocatalytic hydrogen evolution over the initial protonated forms and inorganic–organic derivatives of HLT (**a**) and HNT (**b**) titanates in a bare state and with a Pt cocatalyst as well as platinization increase factors k_{Pt}.

A slope of kinetic curves of hydrogen evolution (Figure 3) indicates that the photocatalytic activity of bare protonated titanates HLT and HNT is very low (φ = 0.01%) and independent of a specific lanthanide. Additional modification of the titanates with Pt nanoparticles, conventionally used as a cocatalyst, allows for facilitating surface charge separation and creating new active sites, decreasing the hydrogen formation overpotential. In our case, the platinization makes the La-containing compound (φ = 0.19%) more than twice as active as the Nd-containing analog (φ = 0.08%). This fact is consistent with earlier reported data on photocatalytic hydrogen evolution from aqueous isopropanol over HLT, HNT and the products of their thermolysis [87] that showed a 2–4 times greater activity of La-containing compounds as compared to Nd-containing ones. However, the activity of both n = 1 titanates proves to be lower than that of their n = 3 counterparts $H_2Ln_2Ti_3O_{10}$ (Ln = La, Nd) under the same conditions [81], which may be associated with the unequal efficiency of charge separation in the perovskite slabs of various thickness (visual comparison of the n = 1 and n = 3 structures is presented in Figure 1).

All the organically modified titanates exhibit much greater hydrogen evolution activity in comparison with their initial protonated forms. At the same time, after the organic modification, the differences in the photocatalytic performance of La- and Nd-containing samples become much more pronounced (Figure 4). These differences might be due to the greater hydratability of the La-containing samples in aqueous media, although the data available do not allow establishing this fact strictly since structure, quantitative composition, chemical properties, light absorption regions and morphology of the compounds with both lanthanides differ slightly [73].

The most active sample in the series of bare n-alkylamine derivatives HLT×RNH_2 is the methylamine titanate (φ = 0.31%); the least activity is shown by ethyl- and n-propylamine compounds (φ = 0.01–0.11%) and intermediate activity values are found for n-butyl-, n-hexyl- and n-octylamine samples (φ = 0.17–0.24%). In the series HNT×RNH_2, the highest photocatalytic activity is demonstrated by the n-propylamine compound (φ = 0.03%), while its values for other derivatives are quite similar (φ = 0.014–0.015%) and practically one order of magnitude lower than for the cognate La-containing hybrid titanates. Platinization greatly changes the correlation of the photocatalytic activity with a specific interlayer amine. In the series HLT×RNH_2/Pt, its maximum relates to the ethylamine-intercalated titanate (φ = 1.3%), which was revealed to be the least active in a bare form. At the same time, the methylamine derivative, being the most active without a cocatalyst, shows the least activity after platinization (φ = 0.65%). Among HNT×RNH_2/Pt representatives, the activity maximum falls on the n-octylamine titanate (φ = 0.38%). The most active sample from each series of bare n-alkoxy derivatives HLT×ROH and HNT×ROH is its simplest representative—methoxy compound (φ = 0.67% for La- and φ = 0.17% for Nd-containing). Further elongation of the grafted n-alkoxy chain results in a sharp activity drop. After platinization, the maximum of the photocatalytic activity in both series HLT×ROH/Pt and HNT×ROH/Pt still falls on the methoxy derivatives (φ = 1.4% for La- and φ = 0.54% for Nd-containing). It should also be noted that while the n-decoxy lanthanum titanate shows a relatively low activity in its series (φ = 0.04% without Pt and φ = 0.33% with Pt), its neodymium counterpart is the second most active after the methoxy compound (φ = 0.12% without Pt and φ = 0.47% with Pt). In general, platinized ethylamine and methoxy derivatives of HLT appear to be the most promising photocatalytic materials among the titanates in question, exhibiting the greatest hydrogen production rate in aqueous methanol.

Thus, the organic modification of the n = 1 titanates allows for improving their hydrogen evolution activity up to 68 times, and the products obtained provide up to 29 times higher apparent quantum efficiency in comparison with the reference photocatalyst TiO_2 P25 Degussa (φ = 0.023% under the same conditions). Having said so, additional surface platinization results in reaching the efficiency up to φ = 1.4%. However, despite the beneficial effect of the organic modification, the photocatalytic performance of the n = 1 titanates turned out to be significantly lower than that of their n = 3 counterparts

$H_2Ln_2Ti_3O_{10}$ tested in our previous report [40]. This trend is especially pronounced upon the platinization: while the $H_2Ln_2Ti_3O_{10}$-based derivatives greatly increase their activity after Pt loading (average k_{Pt} = 20–30), the activity of HLT- and HNT-based ones is generally less dependent on the Pt cocatalyst (k_{Pt} = 5–15) (Figure 4). Moreover, the lowest values of k_{Pt} fall on the most active samples (particularly HLT×MeOH). In view of the above, the photocatalytic performance of HLT- and HNT-based samples, unlike that of $H_2Ln_2Ti_3O_{10}$-based ones, is limited rather by volume electron-hole recombination than by surface one since, otherwise, Pt deposition could have provided a greater effect on the reaction rate. This trend, apparently, originates from the fundamental difference in the structure of the aforementioned n = 3 and n = 1 titanates (Figure 1) since the latter belong to a K_2NiF_4 structural type with a significant difference of the lanthanide surrounding (9-fold coordination in $HLnTiO_4$ instead of 12-fold coordination in $H_2Ln_2Ti_3O_{10}$). Thus, n = 3 structures appear to be preferable for the efficient separation of photogenerated charge carriers than n = 1. A similar trend was observed earlier for n = 2 and n = 3 tantalates [77].

As can be seen from the data presented, the hydrogen evolution activity of the organically modified samples does not show an evident correlation with the organic chain length and, apparently, is associated with the simultaneous influence of several factors. Although the enhanced activity of some derivatives (such as HLT×MeOH and HNT×DcOH) may be associated with their relatively high specific surface area, the surface factor does not explain the experimental trends in the activity in general. A more viable hypothesis explaining the photocatalytic activity increase after organic modification is the functioning of the interlayer space as an additional reaction zone in photocatalysis [45]: inserted organic components expand the interlayer space, facilitating penetration of the reactant molecules to the interlayer reaction centers that are inactive in the unmodified titanates due to the steric limitations. This hypothesis is also supported by the correlation between hydrogen evolution activity and the interlayer water content (Table 1), which was observed earlier for the organically modified n = 3 layered perovskites: as a rule, more hydrated samples exhibit greater activity as compared with the practically anhydrous ones [79–81]. Intercalated water molecules may form highly reactive hydroxyl radicals [90,91] involved in the methanol oxidation along with holes and, thus, increase the hydrogen evolution rate.

The rate of photocatalytic hydrogen evolution from aqueous media is known to depend on their pH [92], although the corresponding correlation in real systems is quite complex because pH may greatly affect the properties of a photocatalyst itself (primarily of its surface). According to our pH measurements (Tables S2 and S3), photocatalytic suspensions of both protonated and *n*-alkoxy compounds are slightly acidic. In the case of the *n*-alkoxy derivatives, it is apparently due to the presence of residual interlayer protons at non-grafted vertices of titanium–oxygen octahedra. The *n*-alkylamine compounds, on the contrary, give slightly alkaline suspensions, and their pH is observed to decline with the amine chain length rising, which may be explained by the lesser propensity of low-polar *n*-alkylamines to transition into the polar aqueous solution. Taking into account the report on the pH influence [92], we could have expected the *n*-alkylamine derivatives to show greater photocatalytic activity since the pH of their suspensions falls in the optimal range of 8–10 (Tables S2 and S3). However, the comparison of their activity with that of most *n*-alkoxy titanates allows considering pH not the main factor determining the differences in their efficiency. Furthermore, the pH of the reaction medium is seen not to stay constant during photocatalytic measurements ($pH_1 \neq pH_2$, Tables S2 and S3). The pH reduction detected during some experiments ($pH_1 > pH_2$) is potentially associated with the partial oxidation of methanol to formic acid. Minor pH increase disclosed for some *n*-alkylamine titanates ($pH_1 < pH_2$) should be due to partial amine deintercalation into the reaction solution.

In the course of preparation of photocatalytic suspensions, it was established that the sample dispersibility is strongly dependent on the polarity of the interlayer organic modifier. Particularly, the titanates modified by short-chain organic components (R = Me, Et, Pr and Bu) readily give suspensions in aqueous methanol under shaking and sonication,

while those containing long-chain interlayer structures (R = Hx, Oc and Dc) do it reluctantly as well as form films on the suspension surface and glass flask because of poor hydratability of low-polar organic chains. Although sonication of the initial protonated titanates is not accompanied by the formation of surface films, their suspensions possess low sedimentation stability without continuous stirring, which may be due to greater particle sizes. Experimental correlations between bare sample concentrations at the beginning (c_1) and at the ending (c_2) of the photocatalytic measurement and specific interlayer organic modifier (Figure S5) show that the most concentrated suspensions are typical of the hybrid compounds with intermediate lengths of *n*-alkylamine or *n*-alkoxy chains. After platinization, concentrations c_1 and c_2, as a rule, reduce due to the probable contraction of the electrical double layer associated with the medium acidification. Despite a perceptible decrease in volume sample concentration during some photocatalytic experiments, an accordant descent of the hydrogen generation rate usually is not seen. This may indicate the proper participation of all sample particles (including those settled on the reaction cell walls) in hydrogen formation.

When interpreting photocatalytic properties of the organically modified layered perovskites, we should take into account their potential exfoliation into nanosheets upon the preliminary sonication or photocatalytic experiments since this may explain the heightened activity of some samples. The presence of nanoparticles may be detected by UV-vis spectrophotometry of the supernatant after moderate centrifugation of the reaction suspensions [40]. In the case of the organically modified titanates in question, the nanoparticle concentration in centrifuged reaction suspensions is quite low (c_3 < 2.0 mg/L). The exceptions are two amine derivatives, HNT×$EtNH_2$ (c_3 = 6.6 mg/L) and HNT×PrNH2 (c_3 = 4.3 mg/L), that, however, do not show abnormally high activity (Figure 4). As revealed earlier, organically modified Ruddlesden–Popper titanates are relatively stable towards exfoliation even under prolonged sonication unless the exfoliating agent (such as TBAOH) is added into the system [40].

2.3. Stability of the Organically Modified Titanates under Photocatalytic Conditions

The stability of the inorganic–organic samples obtained has been examined in two aspects: maintaining the activity during long-term operation and chemical stability of the interlayer organic modifiers.

First of all, the photocatalytic performance of the two most active platinized titanates (HLT×$EtNH_2$/Pt and HLT×MeOH/Pt) was evaluated in the course of several running cycles (Figure S6). It was demonstrated that the samples preserved 85–90% of the initial activity after six cycles with a total duration of 12 h. The photocatalytic nature of hydrogen generation over the organically modified titanates was confirmed by the following evidence. The samples under study do not show dark activity, and after the irradiation source is turned off, all the kinetic curves for hydrogen reach a plateau indicating a zero reaction rate (Figure 3). Furthermore, the hydrogen indeed evolves from the reaction solution rather than from interlayer organic modifiers, which becomes clear from the following calculations. For instance, the hydrogen amount generated over the methoxy derivative HLT×MeOH/Pt during the 12 h photocatalytic measurement (1.2 mmol H_2) exceeds 12.3 times the amount that could have been evolved via the complete oxidation of the interlayer methoxy groups, contained in 25 mg of the irradiated sample (0.0973 mmol H_2). Having said so, the reaction rate stays practically unchanged.

Since some inorganic–organic derivatives of the related *n* = 3 titanates $H_2Ln_2Ti_3O_{10}$, considered in our previous report [81], were found to experience practically complete decomposition of the interlayer organic components during photocatalytic hydrogen generation, similar chemical instability would be expected from the HLT-based samples. However, the *n* = 1 titanates in question turned out to demonstrate significantly greater stability of the interlayer organics under photocatalytic conditions. XRD patterns of the samples separated after photocatalytic measurements (Figure 5) differ from those of the initial compounds by the shift of the (00x) reflections to larger 2θ angles (HLT×$MeNH_2$, HLT×$EtNH_2$), their

widening (HLT×$OcNH_2$, HLT×DcOH) or formation of by-phases (HLT×MeOH). These structural transformations may be caused by the partial degradation of inserted organic modifiers, samples' disordering along the *c* crystallographic axis upon the organic withdrawal, and additional hydration of the interlayer space, respectively. Having said so, unlike the $H_2Ln_2Ti_3O_{10}$-based samples, none of the HLT inorganic–organic derivatives turns structurally into the protonated titanate, which points to at least partial preservation of the interlayer organic components in the course of photocatalysis.

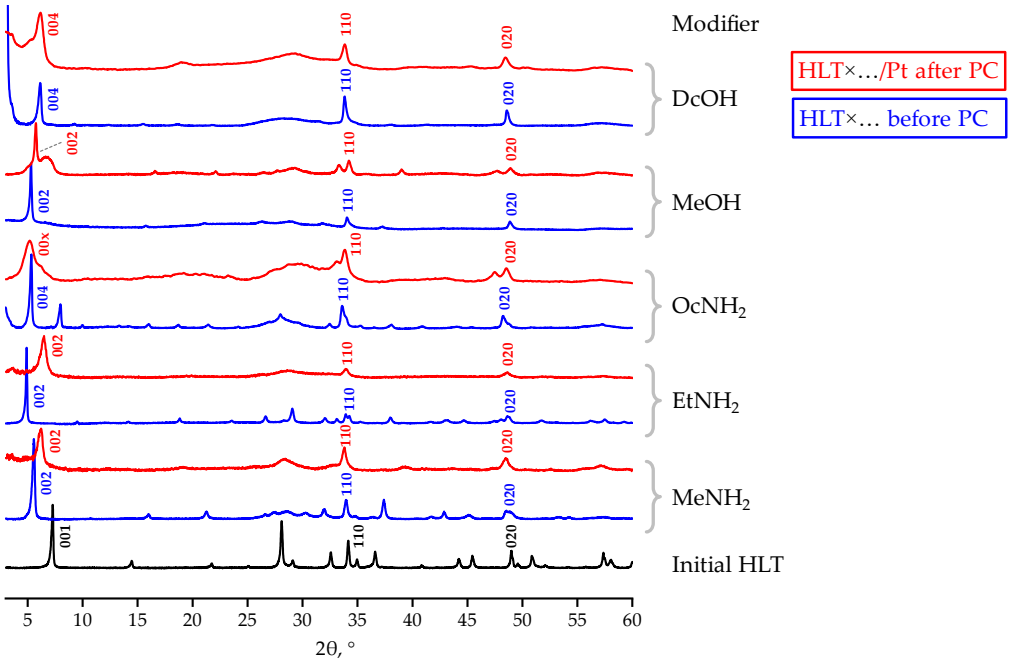

Figure 5. XRD patterns of some inorganic–organic derivatives before and after photocatalytic (PC) experiments.

This fact is fully consistent with the Raman spectra of the final samples (Figure 6) that clearly indicate the presence of organic modifiers in their matrix. However, the relative intensity of some bands diminishes after photocatalytic experiments, which is more pronounced in the case of HLT×$EtNH_2$, HLT×$OcNH_2$ and HLT×DcOH and, apparently, is associated with a decrease in organic content in these samples. At the same time, HLT×$MeNH_2$ and HLT×MeOH taken after photocatalysis show intense vibrational bands of the interlayer organics, comparable with those in the spectra of the initial materials. In accordance with the results of quantitative CHN-analysis, HLT×$MeNH_2$ and HLT×MeOH indeed preserve a vast majority of the organic modifier in the course of photocatalytic measurements: the former contains 0.3 residual methylamine molecules per formula unit (initial content 0.35) and the latter includes 0.5 methoxy groups per formula unit (initial content 0.7). However, the organically modified titanates with longer organic chains (HLT×$EtNH_2$, HLT×$OcNH_2$, HLT×DcOH) appear to preserve only approximately 0.1 organic units per titanate formula whilst the initial content is 0.35–0.45. The estimated compositions of the final samples are in good consistency with total mass losses observed in their TG curves (Figure S7). Being analyzed after photocatalysis, the organically modified titanates exhibit a significantly less pronounced mass gain in the temperature range above 450 °C that is interpreted as partial oxidation of the residual carbon in the sample [73]. This fact points to the probable weakening of the bond between the perovskite matrix and organic component during photocatalysis, which allows the residual organics to liberate at lower temperatures.

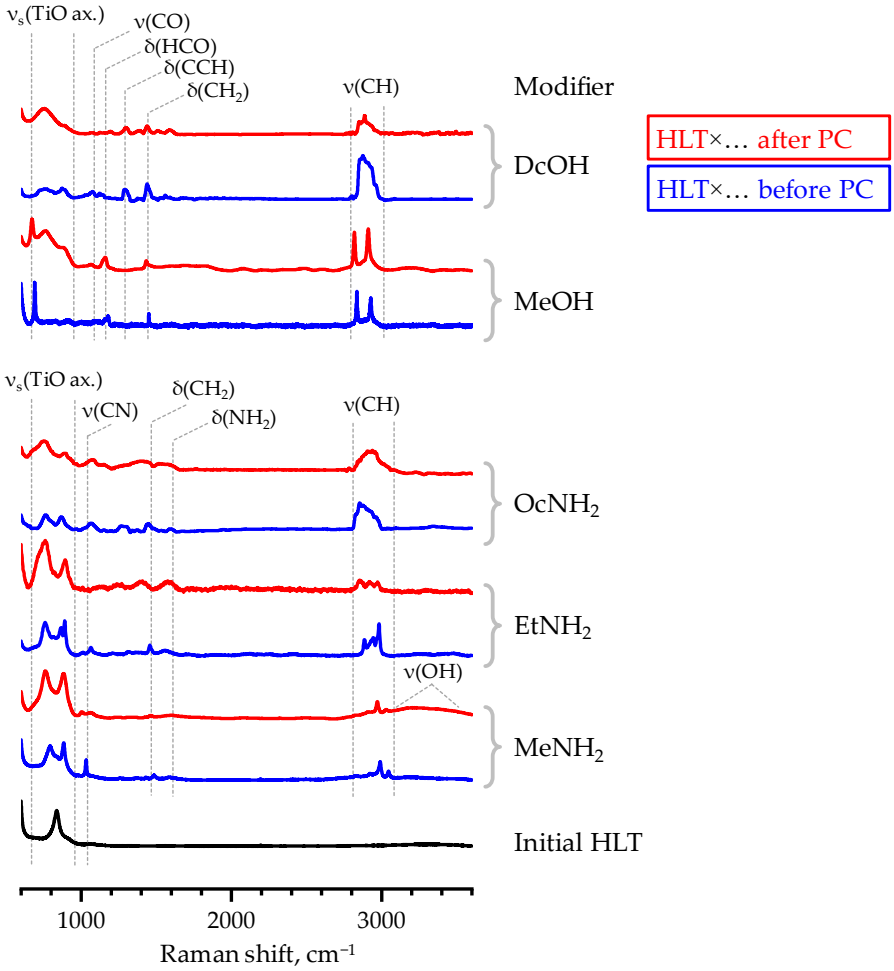

Figure 6. Raman spectra of some inorganic–organic derivatives before and after photocatalytic (PC) experiments.

SEM images of the long-chain inorganic–organic derivatives, separated after photocatalytic experiments (Figure 7), clearly show that the samples undergo pronounced lamination, which is probably caused by the partial withdrawal of long organic components from the interlayer space during photocatalysis. This morphological feature is consistent with the aforementioned reduction of the (00x) XRD peaks since the final samples inevitably become more disordered along the *c* crystallographic axis. Nanoparticles of the Pt cocatalyst are seen in the SEM images as light dots of 5–7 nm in size. The lamination observed not only increases the sample surface but also facilitates the penetration of solution molecules into the interlayer space, increasing the probability of Pt reduction in this zone with the formation of interlayer active sites for hydrogen evolution, although the latter assumption requires a separate experimental verification.

2.4. Possible Interpretations of Photocatalytic Properties of the Organically Modified Titanates

As the study has shown, organic modification of layered perovskite-like titanates HLT and HNT can provide a great increase in their photocatalytic activity with regard to hydrogen production from aqueous methanol. The activity growth may be caused by greater accessibility of the interlayer space, considered an additional reaction zone, for reactants—methanol and water molecules. In other words, interlayer organic modifiers strongly enlarge the interlayer distance *d* and, thus, create new channels for the diffusion of the reactants to the interlayer reaction centers (Figure 8). Along with the reactants, the platinizing agent used, H_2PtCl_6, also might enter the expanded interlayer zone and provide interlayer platinization of the sample. The SEM images (Figure 7) indicate the plausibility

of this hypothesis since one can see Pt nanoparticles located in the region of the crystal lamination, pointing to the possible platinum deposition also in the interlayer space far from the crystal boundaries. Nevertheless, the available data do not allow firm conclusions to be drawn, and the interlayer platinization at the moment remains only a guess requiring further research.

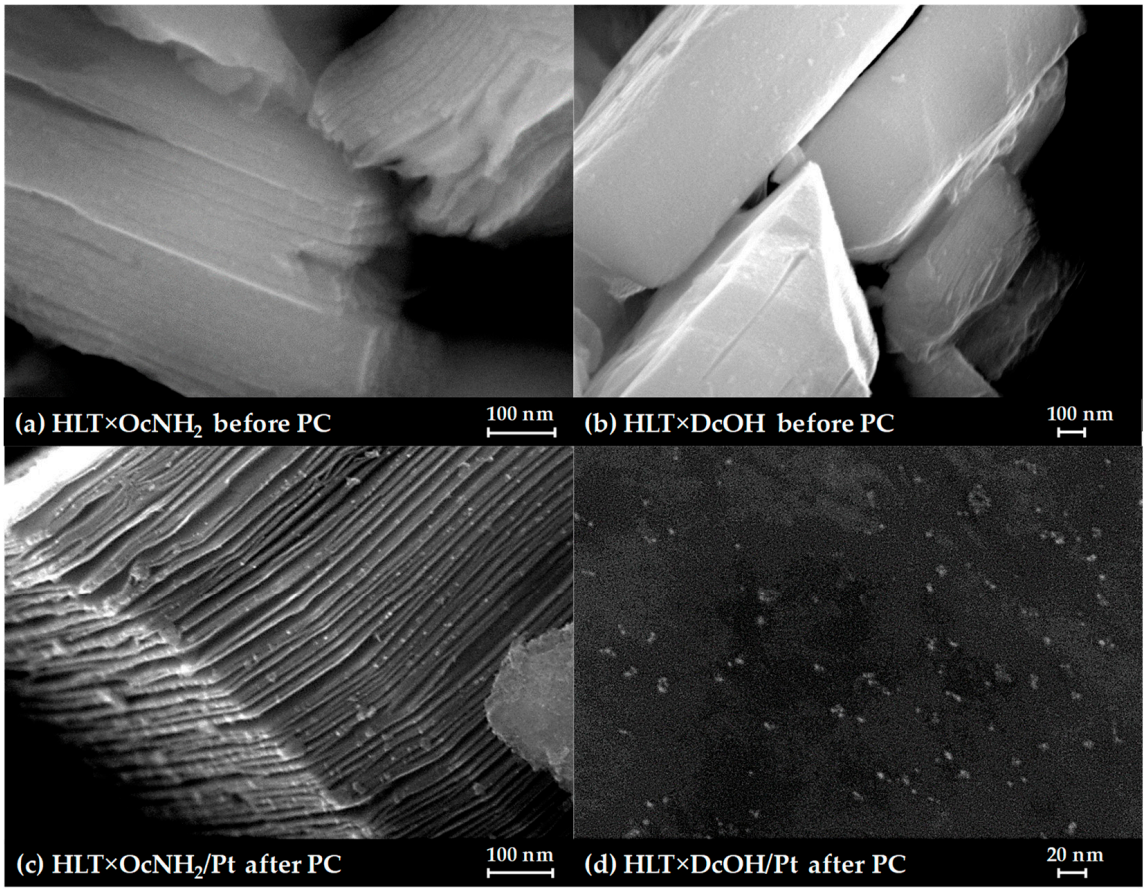

Figure 7. SEM images of the initial *n*-octylamine (**a**) and *n*-alkoxy (**b**) derivatives and their composites with a Pt cocatalyst after the photocatalytic experiment (**c**,**d**).

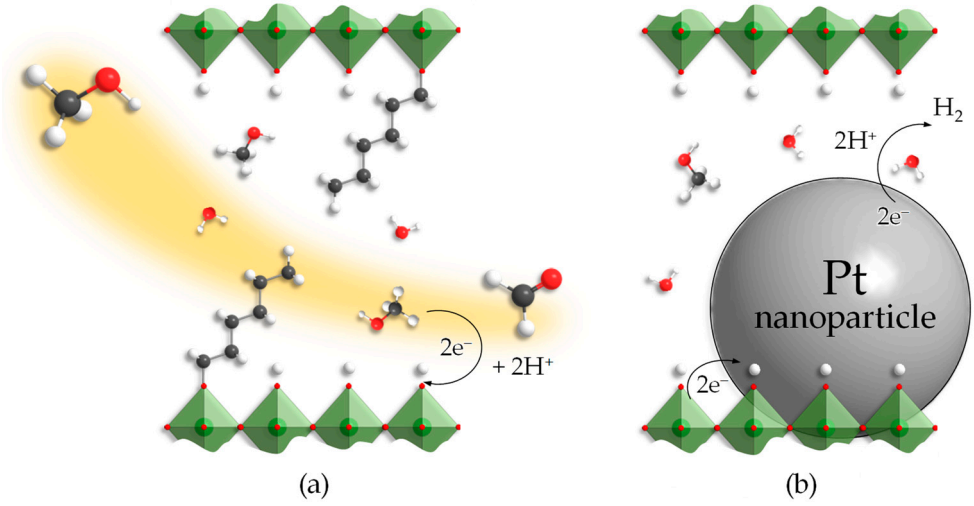

Figure 8. Potential explanations of the photocatalytic properties of inorganic–organic derivatives: increasing of the interlayer reaction zone accessibility (**a**), reduction of Pt nanoparticles in this zone (**b**).

Moreover, the correlation between the photocatalytic activity and interlayer hydration degree indicates that water molecules, apparently, are also involved in the photocatalytic process, despite the presence of easily oxidizable methanol. The role of water molecules probably consists in the formation of reactive hydroxyl radicals providing further oxidation of the alcohol. Organic modifiers may also affect electrosurface properties of the titanates changing constants of reactant adsorption and product desorption as well as offsetting energy band boundaries in near-surface layers, but these issues require a more detailed study. At the same time, the drastic activity rise on moving from the protonated titanates to hybrid inorganic–organic compounds is not due to the band gap contraction, functioning of organic modifiers as photosensitizers, enhancement of crystallinity, exfoliation of the samples into nanosheets or perceptible change in the equilibrium pH value of their reaction suspensions.

Despite the stable hydrogen evolution rate over most samples in question, the interlayer organic modifiers experience partial decomposition during photocatalysis. Thus, the photocatalytic activity observed, strictly speaking, is inherent not in the initial samples taken before loading into the reactor but in the products of their transformations existing under the photocatalytic conditions. Moreover, these products may be stable only in the reaction medium and not amenable to isolating individually.

3. Materials and Methods

3.1. Materials Preparation

All the samples for this photocatalytic study were synthesized in full accordance with the methods from our previous report [73]. In brief, initial alkaline titanates $NaLnTiO_4$ (NLT) were prepared following the conventional ceramic technique. The products obtained were treated with hydrochloric acid to produce their protonated forms HLT and HNT, further used for the preparation of hybrid inorganic–organic derivatives HLT×RNH_2/HNT×RNH_2 and HLT×ROH/HLT×ROH via the intercalation of *n*-alkylamines and grafting of *n*-alcohols into the interlayer space. Brief synthesis conditions are summarized in Table S4.

3.2. Investigation of Photocatalytic Activity

Photocatalytic activity was studied with respect to light-driven hydrogen evolution from 1 mol. % methanol both for bare samples and their composites with a 1% Pt cocatalyst under near-ultraviolet irradiation. The experiments were performed on the laboratory photocatalytic setting used in our previous reports [78–82], presented in Scheme S1. The photocatalytic performance of the samples was evaluated in terms of hydrogen evolution rate ω, apparent quantum efficiency φ and multiplicity of increase in the rate after Pt loading (platinization increase factor k_{Pt}). The method for calculation φ is presented in Information S1.

3.3. Testing the Activity of Bare Samples (No Cocatalyst)

To prepare the reaction suspension, 0.03 g of the sample was placed in a round-bottom flask containing 60 mL of 1 mol. % aqueous methanol. The flask was sealed, shaken and sonicated in an Elmasonic S10H bath (Elma, Singen, Germany) for 10 min. Then, 54 mL of the suspension obtained was pumped into the reaction compartment of the cell, after which the magnetic stirrer, light filter, lamp and argon purging through the suspension were turned on. After 15 min, 4 mL of the suspension was taken from the cell to establish actual volume concentration of the sample and pH of the medium before the photocatalytic measurement (c_1, pH_1). After 15 min, argon purging of the reaction compartment was turned off, and the photocatalytic measurement, consisting of chromatographic analysis of the gaseous phase every 15 min, was conducted for 2 h. Afterwards, the lamp was turned off to organize a 45 min dark stage and monitor potential activity of the sample in the absence of irradiation. Thereafter, 4 mL of the suspension was sampled to determine volume concentration of the sample and pH of the medium at the end of the photocatalytic

measurement (c_2, pH_2). After this, 30 mL of the residual suspension was centrifuged (ELMI CM-6MT (Riga, Latvia)) at a separation factor F = 1000 for 1 h to precipitate bulk particles and determine the concentration of the fine particle fraction in the final colloidal solution as well as its pH value (c_3, pH_3). This step is essential to control the potential formation of perovskite nanosheets via the exfoliation of organically modified samples in the course of photocatalytic measurements since the exfoliation into nanosheets is known to lead to a significant increase in the catalytic activity [65].

3.4. Testing the Activity of Pt-Loaded Samples

In this case, the volume of the initial suspension for pumping into the reaction compartment was 53 mL. Then, 15 min after the magnetic stirrer, light filter, lamp and argon purging were turned on, 1.1 mL of the 1.27 mM H_2PtCl_6 aqueous solution was injected into the reaction suspension to perform in situ photocatalytic platinization of the sample (1 mass. % Pt in the resulting photocatalyst). The gaseous phase was analyzed every 5 min, and the dark stage duration was 20 min. Other experimental conditions and procedures were the same.

3.5. Investigation of Stability under Photocatalytic Conditions

Photocatalytic performance of the most active samples (platinized HLT×$EtNH_2$ and HLT×MeOH) was additionally investigated by conducting several running cycles of hydrogen generation from 1 mol. % aqueous methanol with total duration of 12 h. Chemical stability towards photodegradation of the organic modifiers in the course of photocatalysis was studied for the two aforementioned derivatives and for those with the shortest and the longest organic chain (HLT×$MeNH_2$, HLT×$EtNH_2$, HLT×$OcNH_2$, HLT×MeOH, HLT×DcOH). The samples were separated from the reaction suspension after the standard photocatalytic experiment via vacuum filtering, air-dried and investigated by means of XRD, Raman spectroscopy, TG, CHN-analysis and SEM. The data obtained were compared with those for the initial samples.

3.6. Characterization

3.6.1. XRD

Powder X-ray diffraction (XRD) patterns of the samples were recorded on a Rigaku Miniflex II benchtop diffractometer (Tokyo, Japan) using CuK_α radiation, an angle range 2θ = 3–60° and a scanning rate of 10°/min. The lattice parameters in the tetragonal system were calculated on the basis of all the diffraction peaks observed using DiffracPlus Topas software.

3.6.2. Raman Spectroscopy

Raman scattering spectra were collected on a Bruker Senterra spectrometer (Billerica, MA, USA) in the wavenumber range of 600–3600 cm^{-1}. Protonated titanates, *n*-alkylamine and methoxy derivatives were studied using a 488 nm incident laser (power 4 mW, accumulation time 10 s), *n*-decoxy derivatives—785 nm (power 50 mW, accumulation time 60 s).

3.6.3. DRS

Diffuse reflectance spectra (DRS) were recorded on a Shimadzu UV-2550 spectrophotometer (Kyoto, Japan) with an ISR-2200 integrating sphere attachment in the range of 220–800 nm using barium sulfate as an external reference with the reflection coefficient R = 1. The reflectance spectra were transformed into coordinates $(F \cdot h\nu)^{1/2} = f(h\nu)$, where $F = (1 - R)^2/2R$ is the Kubelka–Munk function. Linear sections of the graph were extrapolated, and an optical bandgap energy E_g was found as an abscissa of their intersection point.

3.6.4. CHN-Analysis

Quantitative compositions of the inorganic–organic derivatives were calculated on the basis of carbon, hydrogen and nitrogen content determined via the elemental CHN analysis on a Euro EA3028-HT analyzer (EuroVector, Pavia, Italy).

3.6.5. TG

Thermogravimetric (TG) analysis was performed on a Netzsch TG 209 F1 Libra thermobalance (Selb, Germany) in the synthetic air atmosphere. The temperature program included heating the sample from room temperature to 900 °C at a rate of 10 °C/min followed by keeping it at the maximum temperature for 20 min to achieve establishing the constant mass.

3.6.6. SEM

Morphology of the samples was studied on a Zeiss Merlin scanning electron microscope (SEM) (Oberkochen, Germany) equipped with a field emission cathode, electron optics column Gemini II and oil-free vacuum system.

3.6.7. BET

Specific surface areas S of the samples were measured by a Micromeritics ASAP 2020 volumetric adsorption analyzer (Norcross, GA, USA). Prior to analysis, 150–200 mg of each sample was degassed for 12 h at 25 °C. Adsorption isotherms were obtained at a liquid nitrogen temperature (−196 °C) with Kr as an adsorptive. Specific surface areas were calculated via the conventional Brunauer-Emmett-Teller method (BET) using at least five points from the relative pressure range of 0.05–0.15. The Kr molecular cross-sectional area was assumed to be 0.210 nm^2.

3.6.8. ICP-AES

Concentrations of the perovskite nanosheet colloidal solutions used for building spectrophotometric calibration plots were determined by inductively coupled plasma atomic emission spectroscopy (ICP-AES) on a Shimadzu ICPE-9000 spectrometer (Kyoto, Japan) after preliminary acid digestion.

3.6.9. Spectrophotometry

Actual volume concentrations c_1, c_2, c_3 of the samples in photocatalytic suspensions were determined via spectrophotometric analysis performed on a Thermo Scientific Genesys 10S UV-vis spectrophotometer (Waltham, MA, USA) using previously built calibration plots (Figure S8). Measurements were conducted in the range of optical density $A < 2$. The 1 mol. % aqueous methanol was used for dilution and baseline subtraction.

3.6.10. pH Measurement

The pH values of the reaction medium were controlled using a laboratory pH-meter Toledo SevenCompact S220 (Greifensee, Switzerland) equipped with an InLab Expert Pro-ISM electrode.

4. Conclusions

In the present article, we have carried out a comprehensive investigation of 24 hybrid inorganic–organic compounds based on layered perovskite-like titanates HLT and HNT as photocatalytically active materials for light-driven hydrogen production from aqueous methanol, a typical biomass-derived alcohol. Organic modification of the titanates' interlayer space by *n*-alkylamines and *n*-alkoxy groups allowed improving the hydrogen evolution activity up to 68 times and obtaining the samples providing up to 29 times higher apparent quantum efficiency in comparison with the reference photocatalyst TiO_2 P25 Degussa. The platinized ethylamine and methoxy derivatives of HLT proved to be the most promising photocatalytic materials among the $n = 1$ organically modified titanates

under study (φ = 1.3–1.4%). The activity was found to correlate with the hydration degree of the interlayer space, considered an additional reaction zone in photocatalysis. It was assumed that organic modification substantially improves the accessibility of this zone for reactants and, potentially, for the platinizing agent, which, apparently, accounts for the multiple activity growth. Moreover, the inorganic–organic derivatives of the $n = 1$ titanates demonstrated significantly greater chemical stability with respect to photodegradation of the interlayer organic components in comparison with the $H_2Ln_2Ti_3O_{10}$-based samples reported earlier. However, the latter allowed reaching an order of magnitude higher quantum efficiency of hydrogen evolution under the same conditions, probably, due to better charge separation in the three-layer ($n = 3$) perovskite slabs as compared with the single-layer ($n = 1$) ones.

Supplementary Materials: The following supporting information can be downloaded at: https://www.mdpi.com/article/10.3390/catal13040749/s1, Information S1: Method for calculation of apparent quantum efficiency; Figure S1: XRD patterns of the initial protonated titanates HLT and HNT and their inorganic–organic derivatives; Figure S2: Diffuse reflectance spectra and Tauc plots for the initial protonated titanates HLT and HNT; Figure S3: Diffuse reflectance spectra and Tauc plots for *n*-alkylamine and *n*-alkoxy derivatives of HLT and HNT; Figure S4: Emission spectrum of the DRT-125 lamp and absorption regions of the samples under study; Figure S5: Comparison of actual volume concentrations of the HLT- and HNT-based samples in reaction suspensions in the beginning and in the ending of the photocatalytic experiment; Figure S6: Hydrogen generation rate from 1 mol. % aqueous methanol over platinized ethylamine and methoxy derivatives of HLT after several running cycles; Figure S7: TG curves of methylamine, ethylamine, *n*-octylamine, methoxy and *n*-decoxy derivatives of HLT before and after photocatalytic (PC) experiments; Figure S8: Spectrophotometric calibration plots for monitoring the volume concentrations of bulk and exfoliated fractions and HLT- and HNT-based samples in the reaction suspensions; Scheme S1: Scheme of photocatalytic setting and reaction cell and their operating principle; Table S1: Photocatalytic activity of the initial protonated titanates and their inorganic–organic derivatives in a bare form and after surface modification with a Pt cocatalyst; Table S2: Actual volume concentrations and pH values of the reaction suspensions of HLT-based samples; Table S3: Actual volume concentrations and pH values of the reaction suspensions of HNT-based samples; Table S4: Conditions for the synthesis of the initial titanates and their inorganic–organic derivatives.

Author Contributions: Conceptualization, O.I.S. and I.A.Z.; methodology, O.I.S., S.A.K. and V.V.V.; investigation, S.A.K. and V.V.V.; data curation, O.I.S. and I.A.R.; writing—original draft preparation, S.A.K. and I.A.Z.; writing—review and editing, S.A.K., O.I.S. and I.A.R.; visualization, S.A.K., V.V.V. and I.A.R.; supervision, I.A.Z. and O.I.S.; funding acquisition, O.I.S. and I.A.Z.; project administration, I.A.Z. All authors have read and agreed to the published version of the manuscript.

Funding: The study was financially supported by the Russian Science Foundation (project No. 22-73-10110—preparation and identification of the organically modified titanates; project No. 19-13-00184—investigation of their photocatalytic activity and stability).

Data Availability Statement: The data presented in this study are available in the article.

Acknowledgments: The study was conducted using the equipment of the Saint Petersburg State University Research Park: Center for X-ray Diffraction Studies, Center for Optical and Laser Research, Center for Chemical Analysis and Materials Research, Center for Thermal Analysis and Calorimetry, Interdisciplinary Center for Nanotechnology and Center for Innovative Technologies of Composite Nanomaterials. This article is dedicated to the 300th anniversary of Saint Petersburg State University.

Conflicts of Interest: The authors declare that they have no known competing financial interest or personal relationships that could have appeared to influence the research reported in this paper.

References

1. Moiseev, I. Green chemistry: Development trajectory. *Russ. Chem. Rev.* **2013**, *82*, 616–623. [CrossRef]
2. Kozlova, A.E.; Parmon, V.N. Heterogeneous semiconductor photocatalysts for hydrogen production from aqueous solutions of electron donors. *Russ. Chem. Rev.* **2017**, *86*, 870–906. [CrossRef]

3. Chen, X.; Zhao, J.; Li, G.; Zhang, D.; Li, H. Recent advances in photocatalytic renewable energy production. *Energy Mater.* **2022**, *2*. [CrossRef]
4. Rozhkova, E.; Ariga, K. *From Molecules to Materials Pathways to Artificial Photosynthesis*; Springer: Berlin/Heidelberg, Germany, 2015.
5. Ismail, A.A.; Bahnemann, D.W. Photochemical splitting of water for hydrogen production by photocatalysis: A review. *Sol. Energy Mater. Sol. Cells* **2014**, *128*, 85–101. [CrossRef]
6. Ahmad, H.; Kamarudin, S.; Minggu, L.; Kassim, M. Hydrogen from photo-catalytic water splitting process: A review. *Renew. Sustain. Energy Rev.* **2015**, *43*, 599–610. [CrossRef]
7. Takanabe, K. Photocatalytic Water Splitting: Quantitative Approaches toward Photocatalyst by Design. *ACS Catal.* **2017**, *7*, 8006–8022. [CrossRef]
8. Jiang, Z.; Ye, Z.; Shangguan, W. Recent advances of hydrogen production through particulate semiconductor photocatalytic overall water splitting. *Front. Energy* **2022**, *16*, 49–63. [CrossRef]
9. Yao, Y.; Gao, X.; Meng, X. Recent advances on electrocatalytic and photocatalytic seawater splitting for hydrogen evolution. *Int. J. Hydrogen Energy* **2021**, *46*, 9087–9100. [CrossRef]
10. Walter, M.G.; Warren, E.L.; McKone, J.R.; Boettcher, S.W.; Mi, Q.; Santori, E.A.; Lewis, N.S. Solar Water Splitting Cells. *Chem. Rev.* **2010**, *110*, 6446–6473. [CrossRef]
11. Christoforidis, K.C.; Fornasiero, P. Photocatalytic Hydrogen Production: A Rift into the Future Energy Supply. *Chemcatchem* **2017**, *9*, 1523–1544. [CrossRef]
12. Puga, A.V. Photocatalytic production of hydrogen from biomass-derived feedstocks. *Coord. Chem. Rev.* **2016**, *315*, 1–66. [CrossRef]
13. Liu, R.; Yoshida, H.; Fujita, S.-I.; Arai, M. Photocatalytic hydrogen production from glycerol and water with NiO_x/TiO_2 catalysts. *Appl. Catal. B Environ.* **2014**, *144*, 41–45. [CrossRef]
14. Taboada, E.; Angurell, I.; Llorca, J. Hydrogen photoproduction from bio-derived alcohols in an optical fiber honeycomb reactor loaded with Au/TiO_2. *J. Photochem. Photobiol. A Chem.* **2014**, *281*, 35–39. [CrossRef]
15. Al-Azri, Z.H.; Chen, W.-T.; Chan, A.; Jovic, V.; Ina, T.; Idriss, H.; Waterhouse, G.I. The roles of metal co-catalysts and reaction media in photocatalytic hydrogen production: Performance evaluation of M/TiO_2 photocatalysts (M = Pd, Pt, Au) in different alcohol–water mixtures. *J. Catal.* **2015**, *329*, 355–367. [CrossRef]
16. Dosado, A.G.; Chen, W.-T.; Chan, A.; Sun-Waterhouse, D.; Waterhouse, G.I. Novel Au/TiO_2 photocatalysts for hydrogen production in alcohol–water mixtures based on hydrogen titanate nanotube precursors. *J. Catal.* **2015**, *330*, 238–254. [CrossRef]
17. Wang, X.; Dong, H.; Hu, Z.; Qi, Z.; Li, L. Fabrication of a $Cu_2O/Au/TiO_2$ composite film for efficient photocatalytic hydrogen production from aqueous solution of methanol and glucose. *Mater. Sci. Eng. B* **2017**, *219*, 10–19. [CrossRef]
18. Li, C.; Wang, H.; Ming, J.; Liu, M.; Fang, P. Hydrogen generation by photocatalytic reforming of glucose with heterostructured CdS/MoS_2 composites under visible light irradiation. *Int. J. Hydrogen Energy* **2017**, *42*, 16968–16978. [CrossRef]
19. Jaswal, R.; Shende, R.; Nan, W.; Shende, A. Photocatalytic reforming of pinewood (Pinus ponderosa) acid hydrolysate for hydrogen generation. *Int. J. Hydrogen Energy* **2017**, *42*, 2839–2848. [CrossRef]
20. Al-Madanat, O.; Curti, M.; Günnemann, C.; AlSalka, Y.; Dillert, R.; Bahnemann, D.W. TiO_2 photocatalysis: Impact of the platinum loading method on reductive and oxidative half-reactions. *Catal. Today* **2021**, *380*, 3–15. [CrossRef]
21. AlSalka, Y.; Al-Madanat, O.; Hakki, A.; Bahnemann, D.W. Boosting the H_2 Production Efficiency via Photocatalytic Organic Reforming: The Role of Additional Hole Scavenging System. *Catalysts* **2021**, *11*, 1423. [CrossRef]
22. Ombaka, L.M.; McGettrick, J.D.; Oseghe, E.O.; Al-Madanat, O.; Best, F.R.G.; Msagati, T.A.; Davies, M.L.; Bredow, T.; Bahnemann, D.W. Photocatalytic H_2 production and degradation of aqueous 2-chlorophenol over B/N-graphene-coated Cu^0/TiO_2: A DFT, experimental and mechanistic investigation. *J. Environ. Manag.* **2022**, *311*, 114822. [CrossRef] [PubMed]
23. Bellardita, M.; García-López, E.I.; Marcì, G.; Palmisano, L. Photocatalytic formation of H_2 and value-added chemicals in aqueous glucose (Pt)-TiO_2 suspension. *Int. J. Hydrogen Energy* **2016**, *41*, 5934–5947. [CrossRef]
24. Zhou, M.; Li, Y.; Peng, S.; Lu, G.; Li, S. Effect of epimerization of D-glucose on photocatalytic hydrogen generation over Pt/TiO_2. *Catal. Commun.* **2012**, *18*, 21–25. [CrossRef]
25. Bahadori, E.; Ramis, G.; Zanardo, D.; Menegazzo, F.; Signoretto, M.; Gazzoli, D.; Pietrogiacomi, D.; Di Michele, A.; Rossetti, I. Photoreforming of Glucose over CuO/TiO_2. *Catalysts* **2020**, *10*, 477. [CrossRef]
26. Bellardita, M.; García-López, E.I.; Marcì, G.; Nasillo, G.; Palmisano, L. Photocatalytic Solar Light H $_2$ Production by Aqueous Glucose Reforming. *Eur. J. Inorg. Chem.* **2018**, *2018*, 4522–4532. [CrossRef]
27. Iervolino, G.; Vaiano, V.; Murcia, J.; Rizzo, L.; Ventre, G.; Pepe, G.; Campiglia, P.; Hidalgo, M.; Navío, J.; Sannino, D. Photocatalytic hydrogen production from degradation of glucose over fluorinated and platinized TiO_2 catalysts. *J. Catal.* **2016**, *339*, 47–56. [CrossRef]
28. Iervolino, G.; Vaiano, V.; Sannino, D.; Rizzo, L.; Ciambelli, P. Production of hydrogen from glucose by $LaFeO_3$ based photocatalytic process during water treatment. *Int. J. Hydrogen Energy* **2016**, *41*, 959–966. [CrossRef]
29. Iervolino, G.; Vaiano, V.; Sannino, D.; Rizzo, L.; Galluzzi, A.; Polichetti, M.; Pepe, G.; Campiglia, P. Hydrogen production from glucose degradation in water and wastewater treated by $Ru\text{-}LaFeO_3/Fe_2O_3$ magnetic particles photocatalysis and heterogeneous photo-Fenton. *Int. J. Hydrogen Energy* **2018**, *43*, 2184–2196. [CrossRef]

30. Zhao, H.; Li, C.-F.; Yong, X.; Kumar, P.; Palma, B.; Hu, Z.-Y.; Van Tendeloo, G.; Siahrostami, S.; Larter, S.; Zheng, D.; et al. Coproduction of hydrogen and lactic acid from glucose photocatalysis on band-engineered $Zn_{1-x}Cd_xS$ homojunction. *iScience* **2021**, *24*, 102109. [CrossRef]
31. Zheng, X.; Wang, X.; Liu, J.; Fu, X.; Yang, Y.; Han, H.; Fan, Y.; Zhang, S.; Meng, S.; Chen, S. Construction of $NiP_x/MoS_2/NiS/CdS$ composite to promote photocatalytic H_2 production from glucose solution. *J. Am. Ceram. Soc.* **2021**, *104*, 5307–5316. [CrossRef]
32. Speltini, A.; Scalabrini, A.; Maraschi, F.; Sturini, M.; Pisanu, A.; Malavasi, L.; Profumo, A. Improved photocatalytic H_2 production assisted by aqueous glucose biomass by oxidized g-C_3N_4. *Int. J. Hydrogen Energy* **2018**, *43*, 14925–14933. [CrossRef]
33. Bai, X.; Hou, Q.; Qian, H.; Nie, Y.; Xia, T.; Lai, R.; Yu, G.; Rehman, M.L.U.; Xie, H.; Ju, M. Selective oxidation of glucose to gluconic acid and glucaric acid with chlorin e6 modified carbon nitride as metal-free photocatalyst. *Appl. Catal. B Environ.* **2022**, *303*, 120895. [CrossRef]
34. Speltini, A.; Romani, L.; Dondi, D.; Malavasi, L.; Profumo, A. Carbon Nitride-Perovskite Composites: Evaluation and Optimization of Photocatalytic Hydrogen Evolution in Saccharides Aqueous Solution. *Catalysts* **2020**, *10*, 1259. [CrossRef]
35. Madriz, L.; Tatá, J.; Carvajal, D.; Núñez, O.; Scharifker, B.; Mostany, J.; Borrás, C.; Cabrerizo, F.M.; Vargas, R. Photocatalysis and photoelectrochemical glucose oxidation on Bi_2WO_6: Conditions for the concomitant H_2 production. *Renew. Energy* **2020**, *152*, 974–983. [CrossRef]
36. Silyukov, O.; Chislov, M.; Burovikhina, A.; Utkina, T.; Zvereva, I. Thermogravimetry study of ion exchange and hydration in layered oxide materials. *J. Therm. Anal. Calorim.* **2012**, *110*, 187–192. [CrossRef]
37. Silyukov, O.I.; Kurnosenko, S.A.; Zvereva, I.A. Intercalation of Methylamine into the Protonated Forms of Layered Perovskite-Like Oxides $HLnTiO_4$ (Ln = La and Nd). *Glas. Phys. Chem.* **2018**, *44*, 428–432. [CrossRef]
38. Kurnosenko, S.A.; Silyukov, O.I.; Mazur, A.S.; Zvereva, I.A. Synthesis and thermal stability of new inorganic-organic perovskite-like hybrids based on layered titanates $HLnTiO_4$ (Ln = La, Nd). *Ceram. Int.* **2020**, *46*, 5058–5068. [CrossRef]
39. Shelyapina, M.G.; Lushpinskaya, I.P.; Kurnosenko, S.A.; Silyukov, O.I.; Zvereva, I.A. Identification of Intercalates and Grafted Organic Derivatives of $H_2La_2Ti_3O_{10}$ by Multinuclear NMR. *Russ. J. Gen. Chem.* **2020**, *90*, 760–761. [CrossRef]
40. Kurnosenko, S.A.; Silyukov, O.I.; Minich, I.A.; Zvereva, I.A. Exfoliation of Methylamine and *n*-Butylamine Derivatives of Layered Perovskite-Like Oxides $HLnTiO_4$ and $H_2Ln_2Ti_3O_{10}$ (Ln = La, Nd) into Nanolayers. *Glas. Phys. Chem.* **2021**, *47*, 372–381. [CrossRef]
41. Shelyapina, M.G.; Silyukov, O.I.; Lushpinskaia, I.P.; Kurnosenko, S.A.; Mazur, A.S.; Shenderovich, I.G.; Zvereva, I.A. NMR Study of Intercalates and Grafted Organic Derivatives of $H_2La_2Ti_3O_{10}$. *Molecules* **2020**, *25*, 5229. [CrossRef]
42. Silyukov, O.; Kurnosenko, S.; Minich, I.; Rodionov, I.; Zvereva, I. Protonated Forms of Layered Perovskite-Like Titanate $NaNdTiO_4$: Neutron and X-ray Diffraction Structural Analysis. *Solids* **2021**, *2*, 265–277. [CrossRef]
43. Rodionov, I.A.; Silyukov, O.I.; Utkina, T.D.; Chislov, M.V.; Sokolova, Y.P.; Zvereva, I.A. Photocatalytic properties and hydration of perovskite-type layered titanates $A_2Ln_2Ti_3O_{10}$ (A = Li, Na, K; Ln = La, Nd). *Russ. J. Gen. Chem.* **2012**, *82*, 1191–1196. [CrossRef]
44. Takata, T.; Furumi, Y.; Shinohara, K.; Tanaka, A.; Hara, M.; Kondo, J.N.; Domen, K. Photocatalytic Decomposition of Water on Spontaneously Hydrated Layered Perovskites. *Chem. Mater.* **1997**, *9*, 1063–1064. [CrossRef]
45. Cui, W.; Liu, L.; Ma, S.; Liang, Y.; Zhang, Z. CdS-sensitized $K_2La_2Ti_3O_{10}$ composite: A new photocatalyst for hydrogen evolution under visible light irradiation. *Catal. Today* **2013**, *207*, 44–49. [CrossRef]
46. Zou, Z.; Ye, J.; Arakawa, H. Substitution effects of In^{3+} by Fe^{3+} on photocatalytic and structural properties of Bi_2InNbO_7 photocatalysts. *J. Mol. Catal. A Chem.* **2001**, *168*, 289–297. [CrossRef]
47. Reddy, V.R.; Hwang, D.W.; Lee, J.S. Effect of Zr Substitution for Ti in $KLaTiO_4$ for Photocatalytic Water Splitting. *Catal. Lett.* **2003**, *90*, 39–43. [CrossRef]
48. Kumar, V.; Govind; Uma, S. Investigation of cation (Sn^{2+}) and anion (N^{3-}) substitution in favor of visible light photocatalytic activity in the layered perovskite $K_2La_2Ti_3O_{10}$. *J. Hazard. Mater.* **2011**, *189*, 502–508. [CrossRef]
49. Zhou, Y.; Wen, T.; Guo, Y.; Yang, B.; Wang, Y. Controllable doping of nitrogen and tetravalent niobium affords yellow and black calcium niobate nanosheets for enhanced photocatalytic hydrogen evolution. *RSC Adv.* **2016**, *6*, 64930–64936. [CrossRef]
50. Kawashima, K.; Hojamberdiev, M.; Chen, S.; Yubuta, K.; Wagata, H.; Domen, K.; Teshima, K. Understanding the effect of partial N^{3-}-to-O^{2-} substitution and H^+-to-K^+ exchange on photocatalytic water reduction activity of Ruddlesden–Popper layered perovskite $KLaTiO_4$. *Mol. Catal.* **2017**, *432*, 250–258. [CrossRef]
51. Hu, Y.; Shi, J.; Guo, L. Enhanced photocatalytic hydrogen production activity of chromium doped lead niobate under visible-light irradiation. *Appl. Catal. A Gen.* **2013**, *468*, 403–409. [CrossRef]
52. Huang, Y.; Li, J.; Wei, Y.; Li, Y.; Lin, J.; Wu, J. Fabrication and photocatalytic property of Pt-intercalated layered perovskite niobates $H_{1-x}LaNb_{2-x}Mo_xO_7$ (x = 0–0.15). *J. Hazard. Mater.* **2009**, *166*, 103–108. [CrossRef]
53. Huang, Y.; Li, Y.; Wei, Y.; Huang, M.; Wu, J. Photocatalytic property of partially substituted Pt-intercalated layered perovskite, $ASr_2Ta_xNb_{3-x}O_{10}$ (A = K, H; x = 0, 1, 1.5, 2 and 3). *Sol. Energy Mater. Sol. Cells* **2011**, *95*, 1019–1027. [CrossRef]
54. Oshima, T.; Wang, Y.; Lu, D.; Yokoi, T.; Maeda, K. Photocatalytic overall water splitting on Pt nanocluster-intercalated, restacked $KCa_2Nb_3O_{10}$ nanosheets: The promotional effect of co-existing ions. *Nanoscale Adv.* **2019**, *1*, 189–194. [CrossRef]
55. Cui, W.; Qi, Y.; Liu, L.; Rana, D.; Hu, J.; Liang, Y. Synthesis of PbS–$K_2La_2Ti_3O_{10}$ composite and its photocatalytic activity for hydrogen production. *Prog. Nat. Sci.* **2012**, *22*, 120–125. [CrossRef]
56. Cui, W.; Guo, D.; Liu, L.; Hu, J.; Rana, D.; Liang, Y. Preparation of $ZnIn_2S_4/K_2La_2Ti_3O_{10}$ composites and their photocatalytic H_2 evolution from aqueous Na_2S/Na_2SO_3 under visible light irradiation. *Catal. Commun.* **2014**, *48*, 55–59. [CrossRef]

57. Saito, K.; Kozeni, M.; Sohmiya, M.; Komaguchi, K.; Ogawa, M.; Sugahara, Y.; Ide, Y. Unprecedentedly enhanced solar photocatalytic activity of a layered titanate simply integrated with TiO_2 nanoparticles. *Phys. Chem. Chem. Phys.* **2016**, *18*, 30920–30925. [CrossRef]
58. Liu, Y.; Zhou, Y.; Lv, C.; Zhang, C.; Jin, X.; Meng, Q.; Chen, G. Construction of 2D-composite $HCa_2Nb_3O_{10}/CaNb_2O_6$ heterostructured photocatalysts with enhanced hydrogen production performance. *New J. Chem.* **2018**, *42*, 681–687. [CrossRef]
59. Zheng, B.; Mao, L.; Shi, J.; Chen, Q.; Hu, Y.; Zhang, G.; Yao, J.; Lu, Y. Facile layer-by-layer self-assembly of 2D perovskite niobate and layered double hydroxide nanosheets for enhanced photocatalytic oxygen generation. *Int. J. Hydrogen Energy* **2021**, *46*, 34276–34286. [CrossRef]
60. Chen, X.; Shen, S.; Guo, L.; Mao, S.S. Semiconductor-based Photocatalytic Hydrogen Generation. *Chem. Rev.* **2010**, *110*, 6503–6570. [CrossRef]
61. Zhang, L.; Wong, K.-H.; Chen, Z.; Yu, J.C.; Zhao, J.; Hu, C.; Chan, C.-Y.; Wong, P.-K. AgBr-Ag-Bi_2WO_6 nanojunction system: A novel and efficient photocatalyst with double visible-light active components. *Appl. Catal. A Gen.* **2009**, *363*, 221–229. [CrossRef]
62. Kim, H.G.; Jeong, E.D.; Borse, P.H.; Jeon, S.; Yong, K.; Lee, J.S.; Li, W.; Oh, S.H. Photocatalytic Ohmic layered nanocomposite for efficient utilization of visible light photons. *Appl. Phys. Lett.* **2006**, *89*, 064103. [CrossRef]
63. Kim, H.G.; Borse, P.H.; Choi, W.; Lee, J.S. Photocatalytic Nanodiodes for Visible-Light Photocatalysis. *Angew. Chem.* **2005**, *117*, 4661–4665. [CrossRef]
64. Zhang, L.; Wang, G.; Xiong, Z.; Tang, H.; Jiang, C. Fabrication of flower-like direct Z-scheme β-Bi_2O_3/g-C_3N_4 photocatalyst with enhanced visible light photoactivity for Rhodamine B degradation. *Appl. Surf. Sci.* **2018**, *436*, 162–171. [CrossRef]
65. Maeda, K.; Mallouk, T.E. Two-Dimensional Metal Oxide Nanosheets as Building Blocks for Artificial Photosynthetic Assemblies. *Bull. Chem. Soc. Jpn.* **2018**, *92*, 38–54. [CrossRef]
66. Gomez-Romero, P.; Sanchez, C. *Functional Hybrid Materials*; Wiley-VCH Verlag GmbH: Weinheim, Germany, 2006.
67. Kickelbick, G. *Hybrid Materials: Synthesis, Characterization, and Applications*; Wiley-VCH Verlag GmbH: Weinheim, Germany, 2007.
68. Mir, S.H.; Nagahara, L.A.; Thundat, T.; Mokarian-Tabari, P.; Furukawa, H.; Khosla, A. Review—Organic-Inorganic Hybrid Functional Materials: An Integrated Platform for Applied Technologies. *J. Electrochem. Soc.* **2018**, *165*, B3137–B3156. [CrossRef]
69. Constantino, V.; Barbosa, C.A.S.; Bizeto, M.; Dias, P.M. Intercalation compounds involving inorganic layered structures. *An. Acad. Bras. Cienc.* **2000**, *72*, 45–50. [CrossRef]
70. Jacobson, A.J.; Johnson, J.W.; Lewandowski, J. Intercalation of the layered solid acid $HCa_2Nb_3O_{10}$ by organic amines. *Mater. Res. Bull.* **1987**, *22*, 45–51. [CrossRef]
71. Tahara, S.; Sugahara, Y. Interlayer Surface Modification of the Protonated Triple-Layered Perovskite $HCa_2Nb_3O_{10}\cdot xH_2O$ with *n*-Alcohols. *Langmuir* **2003**, *19*, 9473–9478. [CrossRef]
72. Tahara, S.; Ichikawa, T.; Kajiwara, G.; Sugahara, Y. Reactivity of the Ruddlesden−Popper Phase $H_2La_2Ti_3O_{10}$ with Organic Compounds: Intercalation and Grafting Reactions. *Chem. Mater.* **2007**, *19*, 2352–2358. [CrossRef]
73. Kurnosenko, S.A.; Voytovich, V.V.; Silyukov, O.I.; Minich, I.A.; Malygina, E.N.; Zvereva, I.A. Inorganic-organic derivatives of layered perovskite-like titanates $HLnTiO_4$ (Ln = La, Nd) with *n*-amines and *n*-alcohols: Synthesis, thermal, vacuum and hydrolytic stability. *Ceram. Int.* **2022**, *48*, 7240–7252. [CrossRef]
74. Wang, C.; Tang, K.; Wang, D.; Liu, Z.; Wang, L.; Zhu, Y.; Qian, Y. A new carbon intercalated compound of Dion–Jacobson phase $HLaNb_2O_7$. *J. Mater. Chem.* **2012**, *22*, 11086–11092. [CrossRef]
75. Aznar, A.J.; Sanz, J.; Ruiz-Hitzky, E. Mechanism of the grafting of organosilanes on mineral surfaces. IV. Phenylderivatives of sepiolite and poly (organosiloxanes). *Colloid Polym. Sci.* **1992**, *270*, 165–176. [CrossRef]
76. Shimada, A.; Yoneyama, Y.; Tahara, S.; Mutin, P.H.; Sugahara, Y. Interlayer surface modification of the protonated ion-exchangeable layered perovskite $HLaNb_2O_7\cdot xH_2O$ with organophosphonic acids. *Chem. Mater.* **2009**, *21*, 4155–4162. [CrossRef]
77. Machida, M.; Mitsuyama, T.; Ikeue, K.; Matsushima, S.; Arai, M. Photocatalytic Property and Electronic Structure of Triple-Layered Perovskite Tantalates, $MCa_2Ta_3O_{10}$ (M = Cs, Na, H, and $C_6H_{13}NH_3$). *J. Phys. Chem. B* **2005**, *109*, 7801–7806. [CrossRef]
78. Rodionov, I.A.; Maksimova, E.A.; Pozhidaev, A.Y.; Kurnosenko, S.A.; Silyukov, O.I.; Zvereva, I.A. Layered Titanate $H_2Nd_2Ti_3O_{10}$ Intercalated with *n*-Butylamine: A New Highly Efficient Hybrid Photocatalyst for Hydrogen Production From Aqueous Solutions of Alcohols. *Front. Chem.* **2019**, *7*, 863. [CrossRef]
79. Voytovich, V.V.; Kurnosenko, S.A.; Silyukov, O.I.; Rodionov, I.A.; Minich, I.A.; Zvereva, I.A. Study of *n*-alkylamine Intercalated Layered Perovskite-Like Niobates $HCa_2Nb_3O_{10}$ as Photocatalysts for Hydrogen Production From an Aqueous Solution of Methanol. *Front. Chem.* **2020**, *8*, 300. [CrossRef]
80. Voytovich, V.; Kurnosenko, S.; Silyukov, O.; Rodionov, I.; Bugrov, A.; Minich, I.; Malygina, E.; Zvereva, I. Synthesis of *n*-Alkoxy Derivatives of Layered Perovskite-Like Niobate $HCa_2Nb_3O_{10}$ and Study of Their Photocatalytic Activity for Hydrogen Production from an Aqueous Solution of Methanol. *Catalysts* **2021**, *11*, 897. [CrossRef]
81. Kurnosenko, S.A.; Voytovich, V.V.; Silyukov, O.I.; Rodionov, I.A.; Kirichenko, S.O.; Minich, I.A.; Malygina, E.N.; Khramova, A.D.; Zvereva, I.A. Photocatalytic Activity of *n*-Alkylamine and *n*-Alkoxy Derivatives of Layered Perovskite-like Titanates $H_2Ln_2Ti_3O_{10}$ (Ln = La, Nd) in the Reaction of Hydrogen Production from an Aqueous Solution of Methanol. *Catalysts* **2021**, *11*, 1279. [CrossRef]
82. Rodionov, I.A.; Gruzdeva, E.O.; Mazur, A.S.; Kurnosenko, S.A.; Silyukov, O.I.; Zvereva, I.A. Photocatalytic Hydrogen Generation from Aqueous Methanol Solution over *n*-Butylamine-Intercalated Layered Titanate $H_2La_2Ti_3O_{10}$: Activity and Stability of the Hybrid Photocatalyst. *Catalysts* **2022**, *12*, 1556. [CrossRef]

83. Kurnosenko, S.A.; Voytovich, V.V.; Silyukov, O.I.; Rodionov, I.A.; Zvereva, I.A. Photocatalytic Hydrogen Production from Aqueous Solutions of Glucose and Xylose over Layered Perovskite-like Oxides $HCa_2Nb_3O_{10}$, $H_2La_2Ti_3O_{10}$ and Their Inorganic-Organic Derivatives. *Nanomaterials* **2022**, *12*, 2717. [CrossRef]
84. Blasse, G. Crystallographic data of sodium lanthanide titanates ($NaLnTiO_4$). *J. Inorg. Nucl. Chem.* **1968**, *30*, 656–658. [CrossRef]
85. Byeon, S.-H.; Yoon, J.J.; Lee, S.O. A New Family of Protonated Oxides $HLnTiO_4$ (Ln= La, Nd, Sm, and Gd). *J. Solid State Chem.* **1996**, *127*, 119–122. [CrossRef]
86. Rodionov, I.; Silyukov, O.; Zvereva, I.A. Study of photocatalytic activity of layered oxides: $NaNdTiO_4$, $LiNdTiO_4$, and $HNdTiO_4$ titanates. *Russ. J. Gen. Chem.* **2012**, *82*, 635–638. [CrossRef]
87. Silyukov, O.I.; Abdulaeva, L.D.; Burovikhina, A.A.; Rodionov, I.A.; Zvereva, I.A. Phase transformations during $HLnTiO_4$ (Ln = La, Nd) thermolysis and photocatalytic activity of obtained compounds. *J. Solid State Chem.* **2015**, *226*, 101–106. [CrossRef]
88. Asahi, R.; Morikawa, T.; Ohwaki, T.; Aoki, K.; Taga, Y. Visible-light photocatalysis in nitrogen-doped titanium oxides. *Science* **2001**, *293*, 269–271. [CrossRef]
89. Kurnosenko, S.A.; Silyukov, O.I.; Zvereva, I.A. Preparation of Porous Particles of Layered Perovskite-Like Titanate $HLaTiO_4$. *Glas. Phys. Chem.* **2020**, *46*, 272–276. [CrossRef]
90. Shibata, H.; Ogura, Y.; Sawa, Y.; Kono, Y. Hydroxyl Radical Generation Depending on O_2 or H_2O by a Photocatalyzed Reaction in an Aqueous Suspension of Titanium Dioxide. *Biosci. Biotechnol. Biochem.* **1998**, *62*, 2306–2311. [CrossRef] [PubMed]
91. Nosaka, Y.; Nosaka, A. Understanding Hydroxyl Radical (·OH) Generation Processes in Photocatalysis. *ACS Energy Lett.* **2016**, *1*, 356–359. [CrossRef]
92. Estahbanati, M.K.; Mahinpey, N.; Feilizadeh, M.; Attar, F.; Iliuta, M.C. Kinetic study of the effects of pH on the photocatalytic hydrogen production from alcohols. *Int. J. Hydrogen Energy* **2019**, *44*, 32030–32041. [CrossRef]